Applied Physics Letters

Ballistic transport in periodically modulated MgZnO/ZnO two-dimensional electron systems

Cite as: Appl. Phys. Lett. **115**, 153101 (2019); https://doi.org/10.1063/1.5121005
Submitted: 22 July 2019 . Accepted: 19 September 2019 . Published Online: 07 October 2019

K. Tanaka, J. Falson, Y. Kozuka, M. Uchida, D. Maryenko, J. T. Ye, Y. Iwasa, A. Tsukazaki, J. H. Smet, and M. Kawasaki

Applied Physics Letters ARTICLE scitation.org/journal/apl

Ballistic transport in periodically modulated MgZnO/ZnO two-dimensional electron systems

Cite as: Appl. Phys. Lett. **115**, 153101 (2019); doi: 10.1063/1.5121005
Submitted: 22 July 2019 · Accepted: 19 September 2019 ·
Published Online: 7 October 2019

K. Tanaka,[1] J. Falson,[2,a)] Y. Kozuka,[3,4] M. Uchida,[1] D. Maryenko,[5] J. T. Ye,[6] Y. Iwasa,[1,5] A. Tsukazaki,[7] J. H. Smet,[2] and M. Kawasaki[1,5]

AFFILIATIONS

[1]Department of Applied Physics and Quantum-Phase Electronics Center (QPEC), University of Tokyo, Tokyo 113-8656, Japan
[2]Max-Planck-Institute for Solid State Research, Heisenbergstrasse 1, 70569 Stuttgart, Germany
[3]Research Center for Magnetic and Spintronic Materials, National Institute for Materials Science, 1-2-1 Sengen, Tsukuba 305-0047, Japan
[4]JST, PRESTO, Kawaguchi, Saitama 332-0012, Japan
[5]RIKEN Center for Emergent Matter Science (CEMS), Wako 351-0198, Japan
[6]Device Physics of Complex Materials, Zernike Institute for Advanced Materials, Nijenborgh 4, 9747 AG Groningen, Netherlands
[7]Institute for Materials Research (IMR), Tohoku University, Sendai 980-8577, Japan

[a)]**Electronic address:** j.falson@fkf.mpg.de

ABSTRACT

We report the fabrication of both antidot lattices and unidirectional stripe patterns upon molecular beam epitaxy grown MgZnO/ZnO heterostructures. The magnetoresistance of these high mobility devices exhibits commensurability oscillations associated with ballistic transport of carriers executing orbital motion within the geometry of the imposed modulation.

The electric transport in disordered semiconductor devices is characterized by drifting Brownian motion of carriers in response to an external electric field. In low disorder two-dimensional electron systems (2DESs), however, carriers can propagate long distances between scattering events at low temperatures. In the clean limit, the distance between scattering events, the mean free path (L) of carriers, can reach magnitudes comparable to the device size, and transport is said to enter the ballistic regime. This introduces a paradigm where the macroscopic electrical characteristics are influenced by the trajectory of carriers through the geometry of the device under study, which in turn reveals quantitative information about the microscopic details of carrier transport.

Here, we report magnetotransport features on MgZnO/ZnO-based 2DES, which are attributed to the ballistic motion of carriers within a periodically modulated electrostatic potential. These "Weiss" oscillations[1] emerge when an externally applied magnetic field (B) induces cyclotron motion of carriers with orbital radii commensurate with the geometry of the imposed periodic electrostatic potential.[2–7]

From a broad perspective, two factors have hindered the exploration of ballistic effects in the field of oxide semiconductors. First, nanostructuring remains a challenge for materials that are resilient to wet-etching techniques and hence require destructive dry-etching techniques.[8–11] Second, the weakly dispersing bands common in d-orbital materials result in a modest L due to a relatively low electron mobility (μ) and heavy effective mass (m^*). Here, we use MgZnO/ZnO heterostructures as they have emerged to host the highest mobility carriers among the oxides[12] and display rich fractional quantum Hall features comparable to the best III-V semiconductor heterostructures.[13,14] The mean free path L, defined as $L = v_F\tau$, with $\tau = \mu m^*/e$ being the transport scattering time and $v_F = \frac{\hbar k_F}{m^*}$ the Fermi velocity, is long ($\approx$5 μm) in this material due to the high μ and modest band mass ($m^* = 0.3m_0$). Here, e is the elementary charge, $\hbar$ is the reduced Planck constant, and $k_F = \sqrt{2\pi n}$ is the Fermi wavevector with n being the charge carrier density. All devices were prepared on $Mg_xZn_{1-x}O$/ZnO ($x \approx 0.02$) heterostructures grown by molecular beam epitaxy on ZnO (0001) substrates.[15,16] The conducting interface is located about

250 nm below the surface for all wafers. The sample characteristics are summarized in Table I with L calculated from the parameters quantified from an unpatterned section of the wafers. We establish fabrication techniques, which impose features with dimensions significantly smaller than L while evidently maintaining pristine quantum transport in the heterostructure. Electrical measurements were performed in a ^{3}He ($T = 500$ mK) or dilution refrigerator ($T = 50$ mK) cryostat with a superconducting magnet coil. Resistivity measurements were carried out using low frequency lock-in techniques.

The magnetotransport studies are performed on a Hall bar geometry, as illustrated in Fig. 1(a). The Hall bar is fabricated either by conventional photolithography followed by argon ion-milling or by scratching the surface of the 2DES-containing wafer with a tungsten needle. The latter technique is very simple and is performed in the following manner. The sample is secured on double-sided tape with a tungsten needle being moved relative to its surface in three spatial dimensions using linear actuators. We control this fine motion via a software interface. The scratched pattern can be determined arbitrarily and is monitored in real-time by viewing the sample surface under a microscope. We have found this technique to be effective in mitigating excess disorder in the 2DES, and hence, it has been employed in other experimental situations.[17–19] Periodic patterns as displayed in the scanning electron microscopy (SEM) images in Figs. 1(b) and 1(c) are defined with the help of electron beam (EB) lithography on top of the Hall bar. They consist of either a square antidot lattice (b) or an antidot lattice where three nearest antidots form an equilateral triangle or unidirectional stripes (c). For ion milled Hall bars, this lithography procedure is executed after defining the Hall bar, whereas it is performed before in the case of needle-defined mesas. All devices contain both patterned and unpatterned regions.

The antidot lattices are defined with positive electron beam resist (ZEP). The surface of the MgZnO/ZnO heterostructure is rather hydrophilic, resulting in poor adhesion between the surface and the resist if no countermeasures are taken. Therefore, Hexamethyldisilazane (HMDS) was deployed as an adhesion promoter for spin coating. The exposed area is subjected to a short session of ion-milling after lithography in order to etch away approximately 100 nm of the MgZnO capping layer. The 2DES is strongly depleted underneath these etched regions, even though the etch depth is still far away from the conducting MgZnO/ZnO interface. The antidot array is, apart from its overall lattice geometry (square or triangular), characterized by two parameters: the spacing between nearest neighbor antidots a and the diameter d of a single antidot.

The unidirectional potential modulation is introduced by defining stripes of negative electron beam resist (TEBN-1) on the sample surface. When the device is cooled, the strain induced by the remaining resist as a result of a difference in the thermal expansion coefficients introduces a potential modulation within the 2DES via the piezoelectric effect.[20–22] We find that the modulation amplitude is large, perhaps due to the large piezoelectric response of ZnO.[23] Importantly, the use of negative resist circumvents the need for the invasive etching procedure above the 2DES area, avoiding additional disorder. The stripe array is characterized by the center-to-center distance a between neighboring stripes and the width of the stripes w.

TABLE I. Summary of samples used in this study.

Sample	μ (cm^2/Vs)	n ($\times 10^{11}$ cm^{-2})	L (μm)
S1	570 000	2.7	4.9
S2	280 000	3.4	2.7
S3	450 000	2.6	3.8

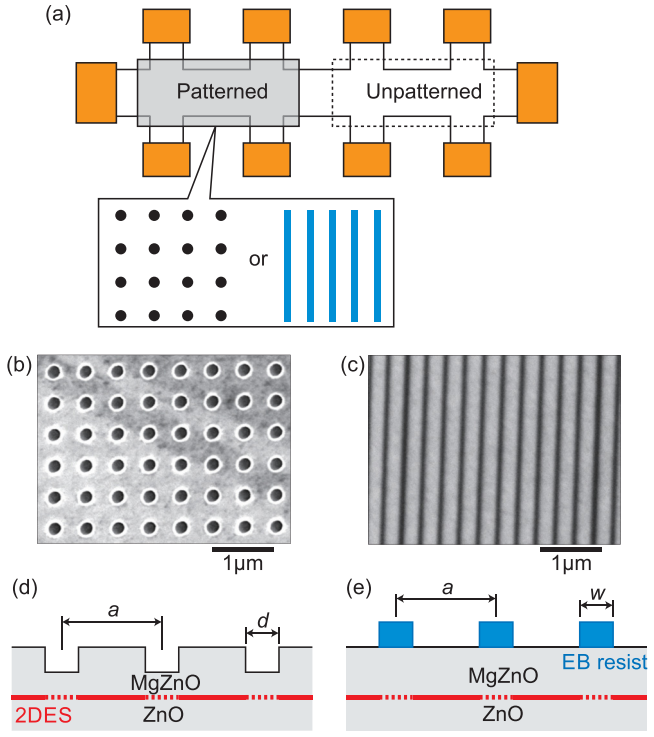

FIG. 1. Device and pattern overview. (a) Schematic of unpatterned and patterned sections of the Hall bar device. The patterned section is modulated by either an antidot or a stripe pattern. The antidot pattern either forms a square or triangular lattice. (b) SEM image of a square antidot lattice. (d) SEM image of a one-dimensional pattern. (e) Cross-sectional schematic of the antidot and stripe patterns. The center-to-center distance of nearest neighbor antidots and the peridoicity of the one-dimensional superlattice are defined as a, whereas d and w are the antidot diameter and stripe width, respectively.

Figure 2 illustrates low field magnetoresistance data in antidot arrays patterned on sample S1 (panel a) and sample S2 (panels b and c). The data in panels (a) and (b) were recorded at 500 mK on square antidot lattices with periodicities a of 500 (a) and 800 nm (b). The nominal antidot diameter equals 200 nm (a) and 80 nm (b), respectively. Shubnikov-de Haas (SdH) oscillations emerge above $B = 0.4$ T. Clear peaks in the sample resistance appear, however, at lower fields on the patterned regions of the sample. Initial models considering steep potential modulations associated these features with the pinning of charge carriers in orbitals commensurate with the superlattice potential, leading to a reduction in conductivity.[5] Later models, however, concluded that chaotic motion of orbitals depinned by an applied electric field within a smooth potential lattice is primarily at play.[24,25] Panel (a) displays a single peak corresponding to the condition where the cyclotron orbit of charge carriers can encompass a single antidot, as schematically shown in the right hand panel. Panel (b) divulges

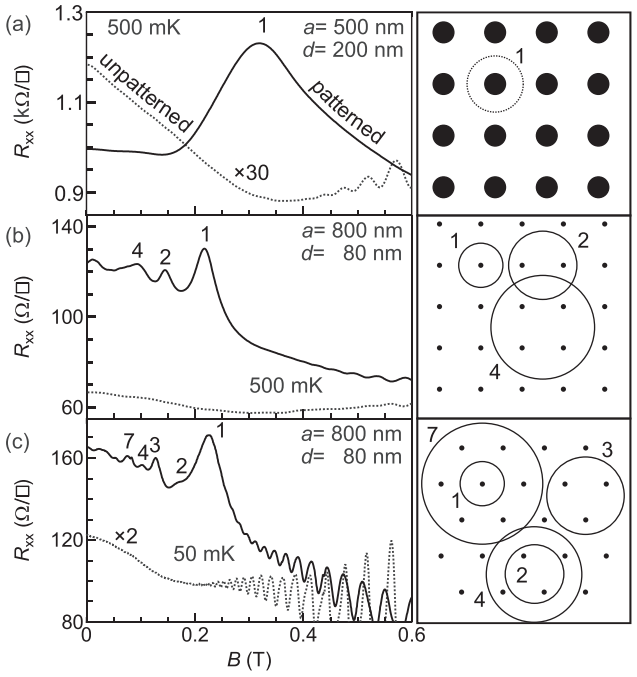

FIG. 2. Magnetotransport through unpatterned (dotted lines) and patterned antidot arrays (solid lines). Panel (a): magnetotransport at $T = 500$ mK for a square antidot lattice with $a = 500$ nm and $d = 200$ nm on sample S1. Panel (b): Magnetotransport at $T = 500$ mK for a square antidot lattice with $a = 800$ nm and $d = 80$ nm on sample S2. Panel (c): Magnetotransport at $T = 50$ mK in a triangular lattice with $a = 800$ nm and $d = 80$ nm on sample S2. Numbers indicated above the peaks in the resistance of the patterned regions correspond to the number of dots enclosed by the orbital motion of carriers as calculated from the classical cyclotron radius. These orbits among the antidot arrays are schematically shown in the right hand side panels.

cleaner transport characteristics owing to the smaller antidot diameter and larger interdot spacing. Features associated with orbital motion around 1, 2, and 4 antidots can be discerned. Panel (c) displays data recorded on a triangular lattice with a nearest neighbor dot spacing of 800 nm and antidot diameter of 80 nm. As a result of the modified lattice geometry in comparison with panel (b), even more commensurability oscillations are resolved.

Figure 3(a) shows low field magnetoresistance data recorded on sample S3 at $T = 500$ mK for a one-dimensional periodic modulation on top of the surface with three different periodicities: $a = 200$ nm, 250 nm, and 300 nm. In all three cases, the stripe width w equals 100 nm. In the unpatterned trace at the bottom of this panel, the Shubnikov-de Haas oscillations begin around $B = 0.4$ T. For a unidirectional potential modulation with a current flow perpendicular to the stripes, the condition for commensurability minima in the longitudinal resistance is given by[1,2]

$$\frac{2R_c}{a} = i - 1/4. \tag{1}$$

Here, $R_c = v_F/\omega_c$ is the cyclotron radius, $\omega_c = eB/m^*$ the cyclotron frequency, and i an integer oscillation index followed by a phase factor. The above expression permits us to predict the B-fields where commensurability minima can be expected, since all these parameters are

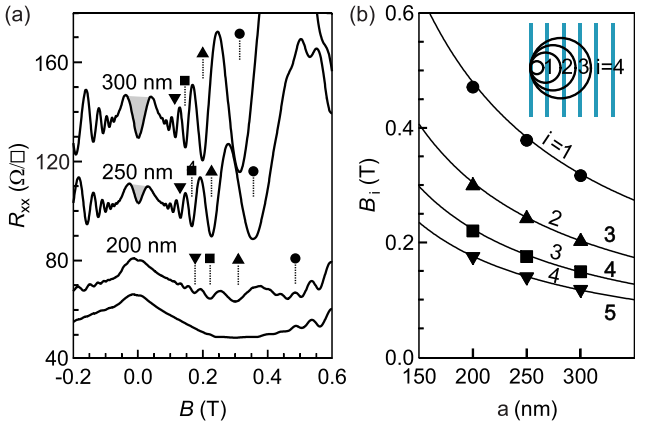

FIG. 3. (a) Magnetotransport through patterned ($a = 300$, 250, and 200 nm) periodic stripe arrays, in comparison with an unpatterned section of sample S3. (b) Magnetic field position of i-th minima (B_i) as a function of a. The inset schematically displays the commensurate orbital motion. Here, $T = 500$ mK.

known or can be extracted (such as, for instance, the density from the Hall resistance to calculate the Fermi velocity).

As seen in Fig. 3(a), the periodic potential indeed induces the expected commensurability oscillations in the patterned sections of the Hall bars only. The inset in panel (b) schematically presents the cyclotron orbits commensurate with the one-dimensional lattice at a resistance minimum. Simple geometric comparisons between L of this device and the calculated R_c suggest that carriers should be able to execute a full cyclotron orbit without scattering for $B \gtrsim 0.05$ T. This is confirmed in experiment, where commensurability oscillations begin to develop at approximately $B \gtrsim 0.07$ T. In panel (a), vertical lines mark the location of the low index commensurability minima as determined with the help of Eq. (1). The agreement with experiment is excellent. Apart from commensurability features, the data also reveal a pronounced positive magnetoresistance (highlighted by gray shading) centered around zero magnetic field before the onset of the commensurability oscillations in lattices of sufficiently large periodicity. A number of models have been proposed to explain this effect. These include magnetic breakdown between minibands produced by the periodic potential,[26] the formation of snake orbits leading to an increase in the drift velocity of carriers parallel to the potential at low B where the Lorentz force provides insufficient momentum to overcome potential barriers,[27] and incomplete cyclotron orbitals due to scattering of carriers before a complete cycle can be completed.[28] Figure 3(b) summarizes the evolution of the observed commensurability oscillation minima with the modulation period. The symbols correspond to the extracted experimental values, and the lines are the calculated positions according to Eq. (1).

The strength of the modulation potential relative to the Fermi energy $\eta = V_0/E_F$ may be obtained through an analysis of the oscillatory contribution $\Delta\rho_{xx}^{osc}$ to the longitudinal resistance. It may be expressed as[22,29,30]

$$\frac{\Delta\rho_{xx}^{osc}}{\rho_0} = A\left(\frac{\pi}{\omega_c\tau_{co}}\right)\frac{\eta^2}{2}\frac{L}{a}A\left(\frac{T}{T_a(B)}\right)\mu B\sin\left(2\pi\frac{2R_c}{a}\right). \tag{2}$$

Here, ρ_0 is the zero field resistivity, $A(x) = x/\sinh(x)$, τ_{co} is the commensurability oscillation lifetime, and $A(T/T_a(B))$ is a thermal

damping factor with $T_a(B) = (ak_F/4\pi^2) \cdot (\hbar\omega_c/k_B)$. This damping factor remains near unity at the measurement temperature of $T = 500$ mK and is therefore neglected in the analysis. Here, k_B is the Boltzmann constant. We estimate η and τ_{co} quantitatively by fitting the envelope of the commensurability oscillations using Eq. (2). For $a = 200$, 250, and 300 nm, we obtain $\eta = 1.4$, 4.8, and 6.7%, while $\tau_{co} = 22$ ps remains approximately constant for all a. The suppression η as a is reduced is due to the smearing of the modulation potential when a is small relative to the distance between the resist pattern on the sample surface and the conducting interface. This trend is in agreement with the results of Ref. 30. The value of η itself is on the upper end of what is reported in the literature[30] and may be due to the strong piezoelectricity of Wurzite ZnO[23] compared to zinc blend III-V semiconductors.[31] The transport lifetime extracted from the zero field resistance equals $\tau_{tr} = 116$ ps. The quantum lifetime estimated from the B-dependence of the SdH oscillations of the unpatterned region is approximately $\tau_q = 4$ ps. It can be deduced from both the amplitude and the onset of the SdH-oscillations. The relation $\tau_q < \tau_{co} < \tau_{tr}$ is similar to what has been reported previously.[30,32,33]

In summary, we have reported pronounced magnetoresistance oscillations associated with the ballistic cyclotron motion of charge carriers within an imposed periodic electrostatic potential in high mobility $Mg_xZn_{1-x}O$/ZnO-based 2DES. This was achieved by patterning either antidot or striped patterns on the top surface of the heterostructures. With further development of the fabrication procedure, we aim to demonstrate similar physics in the fractional quantum Hall regime to study the ballistic motion of composite fermions.[34,35]

We thank Mansour Shayegan for discussions. We acknowledge the financial support of JST CREST Grant No. JPMJCR16F1, Japan. Y.K. acknowledges JST, PRESTO Grant No. JPMJPR1763, Japan. J.F. acknowledges support from the Max Planck—University of British Columbia—University of Tokyo Center for Quantum Materials and the Deutsche Forschungsgemeinschaft (DFG) (No. FA 1392/2-1).

REFERENCES

[1]D. Weiss, K. V. Klitzing, K. Ploog, and G. Weimann, Europhys. Lett. **8**, 179 (1989).
[2]R. R. Gerhardts, D. Weiss, and K. v Klitzing, Phys. Rev. Lett. **62**, 1173 (1989).
[3]R. W. Winkler, J. P. Kotthaus, and K. Ploog, Phys. Rev. Lett. **62**, 1177 (1989).
[4]C. W. J. Beenakker, Phys. Rev. Lett. **62**, 2020 (1989).
[5]D. Weiss, M. L. Roukes, A. Menschig, P. Grambow, K. von Klitzing, and G. Weimann, Phys. Rev. Lett. **66**, 2790 (1991).
[6]T. Yamashiro, J. Takahara, Y. Takagaki, K. Gamo, S. Namba, S. Takaoka, and K. Murase, Solid State Commun. **79**, 885 (1991).
[7]S. Ishizaka, F. Nihey, K. Nakamura, J. i Sone, and T. Ando, Phys. Rev. B **51**, 9881 (1995).
[8]C. W. Schneider, S. Thiel, G. Hammerl, C. Richter, and J. Mannhart, Appl. Phys. Lett. **89**, 122101 (2006).
[9]N. Banerjee, M. Huijben, G. Koster, and G. Rijnders, Appl. Phys. Lett. **100**, 041601 (2012).
[10]A. M. R. V. L. Monteiro, D. J. Groenendijk, N. Manca, E. Mulazimoglu, S. Goswami, Y. Blanter, L. M. K. Vandersypen, and A. D. Caviglia, Nano Lett. **17**, 715 (2017).
[11]H. Hou, Y. Kozuka, J.-W. Liao, L. W. Smith, D. Kos, J. P. Griffiths, J. Falson, A. Tsukazaki, M. Kawasaki, and C. J. B. Ford, Phys. Rev. B **99**, 121302 (2019).
[12]J. Falson, Y. Kozuka, J. H. Smet, T. Arima, A. Tsukazaki, and M. Kawasaki, Appl. Phys. Lett. **107**, 082102 (2015).
[13]J. Falson, D. Maryenko, B. Friess, D. Zhang, Y. Kozuka, A. Tsukazaki, J. H. Smet, and M. Kawasaki, Nat. Phys. **11**, 347 (2015).
[14]J. Falson, D. Tabrea, D. Zhang, I. Sodemann, Y. Kozuka, A. Tsukazaki, M. Kawasaki, K. von Klitzing, and J. H. Smet, Sci. Adv. **4**, eaat8742 (2018).
[15]J. Falson, Y. Kozuka, M. Uchida, J. H. Smet, T. Arima, A. Tsukazaki, and M. Kawasaki, Sci. Rep. **6**, 26598 (2016).
[16]J. Falson and M. Kawasaki, Rep. Prog. Phys. **81**, 056501 (2018).
[17]Y. Matsubara, K. Takahashi, M. Bahramy, Y. Kozuka, D. Maryenko, J. Falson, A. Tsukazaki, Y. Tokura, and M. Kawasaki, Nat. Commun. **7**, 11631 (2016).
[18]Q. Shi, M. A. Zudov, J. Falson, Y. Kozuka, A. Tsukazaki, M. Kawasaki, K. von Klitzing, and J. Smet, Phys. Rev. B **95**, 041411 (2017).
[19]Q. Shi, J. Falson, M. A. Zudov, Y. Kozuka, A. Tsukazaki, M. Kawasaki, and J. Smet, Phys. Rev. B **96**, 125401 (2017).
[20]E. Skuras, A. R. Long, I. A. Larkin, J. H. Davies, and M. C. Holland, Appl. Phys. Lett. **70**, 871 (1997).
[21]I. A. Larkin, J. H. Davies, A. R. Long, and R. Cuscó, Phys. Rev. B **56**, 15242 (1997).
[22]A. Endo, S. Katsumoto, and Y. Iye, Phys. Rev. B **62**, 16761 (2000).
[23]M. Catti, Y. Noel, and R. Dovesi, J. Phys. Chem. Solids **64**, 2183 (2003).
[24]R. Fleischmann, T. Geisel, and R. Ketzmerick, Phys. Rev. Lett. **68**, 1367 (1992).
[25]D. Weiss, K. Richter, E. Vasiliadou, and G. Lütjering, Surf. Sci. **305**, 408 (1994).
[26]P. Steda and A. H. MacDonald, Phys. Rev. B **41**, 11892 (1990).
[27]P. H. Beton, E. S. Alves, P. C. Main, L. Eaves, M. W. Dellow, M. Henini, O. H. Hughes, S. P. Beaumont, and C. D. W. Wilkinson, Phys. Rev. B **42**, 9229 (1990).
[28]A. Endo and Y. Iye, Phys. Rev. B **72**, 235303 (2005).
[29]F. M. Peeters and P. Vasilopoulos, Phys. Rev. B **46**, 4667 (1992).
[30]D. Kamburov, H. Shapourian, M. Shayegan, L. N. Pfeiffer, K. W. West, K. W. Baldwin, and R. Winkler, Phys. Rev. B **85**, 121305 (2012).
[31]A. Beya-Wakata, P.-Y. Prodhomme, and G. Bester, Phys. Rev. B **84**, 195207 (2011).
[32]J. P. Lu and M. Shayegan, Phys. Rev. B **58**, 1138 (1998).
[33]D. Kamburov, M. Shayegan, L. N. Pfeiffer, K. W. West, and K. W. Baldwin, Phys. Rev. Lett. **109**, 236401 (2012).
[34]J. K. Jain, *Composite Fermions* (Cambridge University Press, 2007).
[35]W. Kang, H. L. Stormer, L. N. Pfeiffer, K. W. Baldwin, and K. W. West, Phys. Rev. Lett. **71**, 3850 (1993).